International Journal of Applied Earth Observations and Geoinformation 116 (2023) 103155

Contents lists available at ScienceDirect

International Journal of Applied Earth Observation and Geoinformation

journal homepage: www.elsevier.com/locate/jag

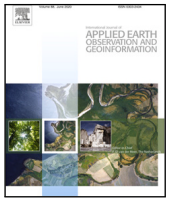

Calculation and restoration of lost spatial information in division-of-focal-plane polarization remote sensing using polarization super-resolution technology

Dong Yao [a,d,*], Hangang Liang [a,c,d], Juan Campos [b], Lei Yan [e], Chunhui Yan [a,d], Chunming Jiang [a,c,d], Songnian Tan [a,d], Chao Liang [a,d], Hanyu Wang [a,d], Lingtong Meng [a,d], Yanping Cheng [a,d]

[a] Changchun Institute of Optics, Fine Mechanics and Physics, Chinese Academy of Science, Changchun, 130033, China
[b] Departament de Física, Universitat Autònoma de Barcelona, Bellaterra, 08193, Spain
[c] University of Chinese Academy of Sciences, Beijing, 100049, China
[d] Key laboratory of Airborne Optical Imaging and Measurement, Chinese Academy of Sciences, Changchun, 130033, China
[e] School of Earth and Space Sciences, Peking University, Beijing, 100871, China

ARTICLE INFO

Keywords:
Polarization remote sensing
Super-resolution
Calibration method
Effect evaluation
Division-of-focal-plane

ABSTRACT

Spatial resolution plays a crucial role in the process of polarization remote sensing method for Earth observation, and the problem of resolution improvement has always been an important research direction in the field of remote sensing. To address the spatial resolution loss and information errors in division-of-focal-plane (DoFP) polarization remote sensing systems, this study proposes a new polarization super-resolution (PSR) remote sensor and a data recovery method. We calibrate the relative displacement between image plane and detector in the laboratory, and verify the effectiveness of this method by actual external imaging. The experimental results demonstrate that the system can eliminate the spatial resolution loss caused by the DoFP technology, and the real image resolution is doubled in both the horizontal and vertical directions. We also verify the effectiveness of this new instrument and data recovery method. By comparing the results of this method with the existing algorithms, it is found that it has a great improvement under the same evaluation parameters, and the texture features of the target scene were significantly enhanced. Moreover, the system can simultaneously perceive multidimensional information, such as high-resolution intensity images and pixel-level polarization information of the target scene, and therefore, can potentially be applied in remote sensing systems.

1. Introduction

Remote sensing involves the acquisition of data from a target, without any physical contact with the target, and the subsequent interpretation of the collected data (Egan, 1992). In polarization remote sensing, the polarization characteristics of a target-scene image are examined to assess a long-distance target.

Along with light intensity, frequency, phase, and polarization are primary physical characteristics of electromagnetic waves. Light photons, after being reflected from objects, exhibit special polarization characteristics that aid in the identification of targets. The perception of polarization characteristics is also the product of natural evolution, and many animals have evolved with polarization sensitivity (Altaqui et al., 2021; Sweeney et al., 2003; Labhart, 1988; Lythgoe and Hemmings, 1967; Cronin et al., 2003). The polarization parameters of light, accompanied with intensity and color, are vital for the development of improved image recognition systems (Wolff, 1997). Polarization images display the shape, surface roughness (Iannarilli Jr. et al., 2000; Aron and Gronau, 2005), and texture (Lillie et al., 1977) information of the objects. Thus, compared with the traditional imaging techniques, polarization imaging technology is more advantageous and can be readily applied in atmospheric remote sensing (Cairns et al., 2003), military reconnaissance (Goldstein, 2000), Ad Astra (Graps and Lane, 1986), and medical diagnosis (Jacques et al., 2002; Liu et al., 2012). Born (Born and Wolf, 2013) as well as Aron and Gronau (2005) introduced the definition of polarization imaging in detail.

Polarization imaging sensors can be classified into division-of-time (Walraven, 1981; Solomon, 1981), division-of-amplitude (Azzam, 1985;

* Corresponding author at: Changchun Institute of Optics, Fine Mechanics and Physics, Chinese Academy of Science, Changchun, 130033, China.
E-mail address: yaodong@ciomp.ac.cn (D. Yao).

https://doi.org/10.1016/j.jag.2022.103155
Received 10 October 2022; Received in revised form 8 December 2022; Accepted 11 December 2022
Available online 22 December 2022

Farlow et al., 2002; Barter et al., 1997; Kudenov et al., 2009), division-of-aperture (Roche et al., 2010; Pezzaniti and Chenault, 2005), and division-of-focal-plane (DoFP) polarimeters (Gruev et al., 2010a; Perkins and Gruev, 2010; Gruev et al., 2010b; Momeni and Titus, 2006; Tyo, 2006; Sarkar et al., 2010; Nordin et al., 1999; Harnett and Craighead, 2002). With the development of nanotechnology and nano-manufacturing, polarization imaging sensors used in visible spectrum known as division-of-focal-plane (DoFP) polarimeters are gradually studied and applied (Gruev et al., 2010a; York and Gruev, 2012). DoFP polarimeters is widely used as it allows real-time imaging. In 2018, Sony introduced the focal-plane-polarization sensing complementary metal-oxide semiconductor imaging sensor chip IMX250MZR, which became the core device in the field of polarization sensing. This chip popularized the use of polarization sensing technology in industry (Atkinson et al., 2021) as well as in real-time sky polarized light navigation (Zhang et al., 2019a). DoFP polarimeters are characterized by an efficient polarization information extraction, a short imaging time (snapshot polarization image information acquisition), small sizes, and high efficiencies. However, the focal-plane-polarization detector collects four linear-polarization-sensing pixel units with angle of 0°, 45°, 90°, and 135° in a group of four adjacent pixels, which greatly reduces the spatial resolution of the original optical system. Because spatial resolution plays an important role in optical remote sensing, the loss of spatial resolution limits the application of polarization imaging.

How can we effectively understand our world with higher resolution technology? Super-resolution (SR) technology can improve the spatial resolution of images, which is of great significance to remote sensing and microscopic measurements, and it is mainly used in the field of microscopic imaging (LotharSchermelleh et al., 2019; Valli et al., 2021). In recent years, some scholars have used SR technology in infrared imaging as well (Zhang et al., 2019b; Chen et al., 2021). With the vigorous development of its learning technology, remote sensing SR technology based on machine learning has also made great progress (Zeng et al., 2019b,a).

In the polarization remote sensing area, researchers have also proposed a series of SR reconstruction methods, which can be roughly divided into interpolation-based and machine learning-based methods. Interpolation-based methods (Ratliff et al., 2009; Tyo et al., 2009; Gao and Gruev, 2011, 2012; Zhang et al., 2017) need to design interpolation rules, and most of them are based on adjacent data of the same polarization state, which has an insurmountable limitation for the improvement of image quality. In the year 2011, Shengkui Gao and Viktor Gruev proposed Bilinear and bicubic interpolation methods for DoFP polarimeters. And then in 2013, they proposed the Gradient-based interpolation method for DoFP polarimeters (Gao and Gruev, 2013). In the year 2016, Junchao Zhang et al. proposed image interpolation for DoFP polarimeters with intensity correlation method (Zhang et al., 2016). In recent years, researchers try to use deep-learning technology to recover high special resolution (Zeng et al., 2019b). Some scholars have proposed a customized polarization demosaicing convolutional neural network (PDCNN) to address the polarization image demosaicing issue (Zhang et al., 2018), which essentially calculates and fills in the unmeasured information. Some scholars have proposed an "end-to-end" all-convolution neural network model-ForkNet. This method cannot give four sub-polarization images of 0°, 45°, 90°, or 135°, which limits its application in scenes such as "de-shining" and "de-fogging". However, the measurement of polarization characteristics is a quantitative process, and there exists an inevitably error between the values obtained by calculation and the actual measurement data, and it is also inevitable that information will be lost in this process.

Therefore, in this study, a microscanning SR technology is applied to optical imaging-based remote sensing, and a polarization-based SR remote sensing imaging system was constructed. Herein, we explain the data recovery method that is used to verify the spatial-resolution restoration accuracy of the DoFP polarization detector. This improve imaging method addresses the problems associated with existing systems such as loss of spatial resolution, polarization information interpretation error, and effectively limits the volume and weight of the system.

The method proposed by the article has three advantages:

1. The basic image data of 0°, 45°, 90°, and 135° are retained. This is very important in some scenes, such as de-fogging scenes, de-shining scenes, and others.

2. The spatial resolution of basic image data are doubled. Spatial resolution is very important for human recognition, and higher resolution means more information.

3. The polarization information error caused by the calculation of adjacent pixels is eliminated. This is beneficial to use polarization information in the field of artificial intelligence identification.

2. Polarization-based SR imaging method

2.1. Basic principle of the DoFP polarization detector

The Stokes vector is defined as Eqs. (1).

$$S = \left[S_0, S_1, S_2, S_3\right]^T = \begin{bmatrix} \frac{1}{2}(I(0°,0°) + I(45°,0°) + I(90°,0°) + I(135°,0°)) \\ I(0°,0°) - I(90°,0°) \\ I(45°,0°) - I(135°,0°) \\ I(0°,90°) - I(0°,-90°) \end{bmatrix} \tag{1}$$

In the above formula, the expression I(a,b) is the irradiance under certain parameters, the parameter a represents the angle between the polarization direction and the specified zero direction (X positive direction) under the detector coordinate system; b indicates the phase delay of the vibrational component in the Y direction relative to the X component after the incoming polarized light is decomposed into X and Y directions under the detector coordinate system. S is called Stokes Vector, S_0, S_1, S_2, and S_3 are called Stokes parameters, S_0 is entire irradiance. S_1 is the difference between irradiance after a 0° and a 90° polarizer. S_2 is the difference between irradiance after a 45° and a 135° polarizer. S_3 is the difference between irradiance after a 0° polarizer and a 90° phase delay, and irradiance after a 0° polarizer and a −90° phase delay, which is equal to the difference of left-handed and right-handed circularly polarized light irradiance.

The degree of linear polarization (Dolp) can be expressed as follows.

$$DoLP = \frac{\sqrt{S_1^2 + S_2^2}}{S_0} \tag{2}$$

The focal plane polarization detector is similar to an RGB (i.e., red (R), blue (B), and green (G)) color detector, except that the band-pass filter is replaced with micro-polarizers with different polarization directions, as shown in Fig. 1.

2.2. Loss of spatial resolution in the polarization process

Micro-polarizers with different polarization directions are considered to be spatially arranged at different intervals, implying that the micro-polarizers in each direction are discontinuous in space. When a sub-image with one of the polarization directions (0°, 45°, 90°, or 135°) is extracted from the original image, the spatial resolution of the sub-image is half in each direction, relative to the original one, as shown in Fig. 2. The image obtained by using the DoFP polarization sensor in one snapshot containing different polarization. Fig. 3 shows the extracted image with 0°, 45°, 90°, or 135° sub-polarization directions. The number of pixels in each sub-image is reduced to one-fourth of that in the original, and therefore, the spatial frequency is reduced to half in each direction.

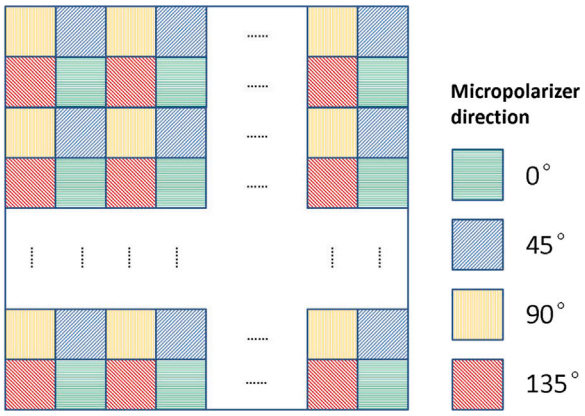

Fig. 1. Schematic of the spatial distribution of the polarization detector pixels. (For interpretation of the references to color in this figure legend, the reader is referred to the web version of this article.)

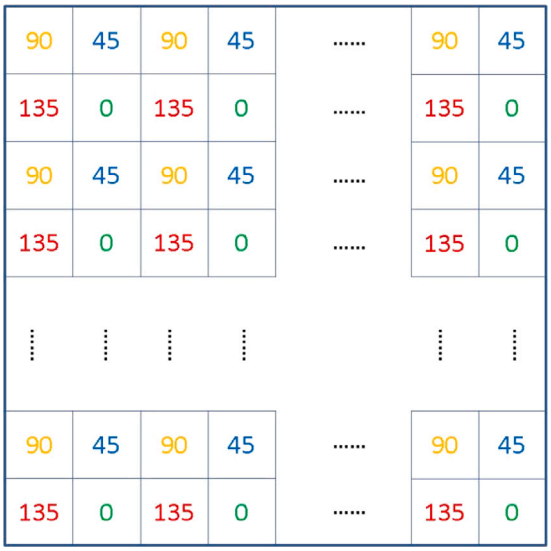

Fig. 2. Original image with four-direction polarization information obtained in one integration time duration.

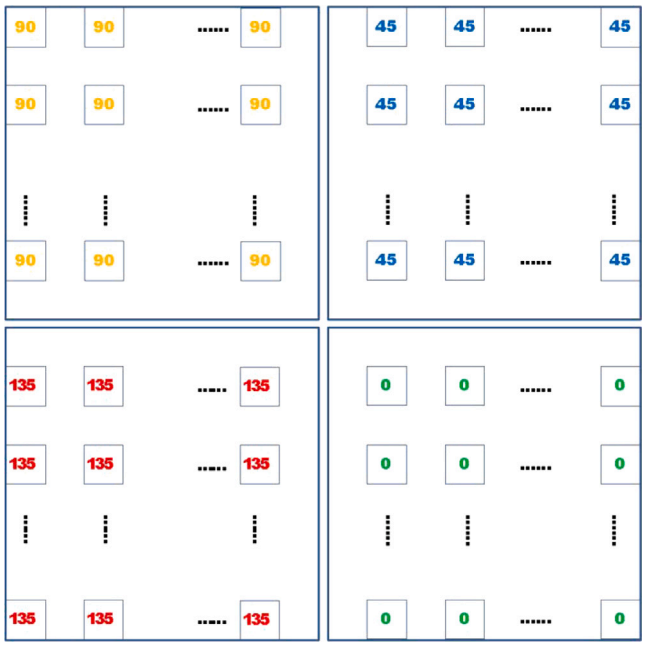

Fig. 3. Spatial resolution of the decomposed image in the sub-polarization direction is reduced to half in each direction relative to the original image.

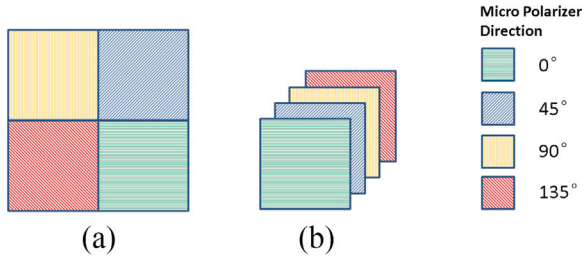

Fig. 4. Two types of target spatial polarization measurement data composition.

2.3. Spatial-separation-induced error in polarization information calculation

When calculating the distribution of polarization information (such as Dolp), the light intensity values of the adjacent four pixels are often used as the basic data, as shown in Fig. 4(a). However, the adjacent four values correspond to different spatial positions. As the polarization in the target scene changes spatially, the four pixels correspond to different spatial polarization information, so any polarization information obtained with this scheme will have errors. On the premise of accurate measurement, this approximation may result in a significant deviation. Ideally, the measurements corresponding to the different orientations of the polarization analyzers should be done at the same spatial location, as shown in Fig. 4(b), which represents the right data composition of the four polarization directions in the same space.

2.4. Proposed polarization SR

2.4.1. Definition of polarization SR

We believe that polarization information is actually a quantitative description of the target scene, and the acquisition of quantitative information requires actual measurement. Therefore, it is difficult to restore the real information of the measured physical space either by rule-based interpolation or by machine learning, and the information gap caused by the lack of original data cannot be made up artificially. Based on the aforementioned considerations, we propose high spacial frequency data recovery method, and in order to better illustrate this method, we also introduce a polarization SR remote sensing system.

To reach the true polarization SR information, the obtained data should meet the following principles:

1. All the three-fourth information lost in the four full-resolution sub-polarization images of 0°, 45°, 90°, or 135° should be measured.
2. Each pixel value of the full-resolution polarization information image should be calculated based on the real measurement data.

The correct restored result should be as shown in Fig. 5.

The SR restoration process of the polarization image that satisfies the aforementioned requirements eliminate the spatial deviation introduced by adjacent pixels, and therefore, obtains better polarization resolution accuracy, and SR in spatial resolution. This information restores the true polarization information of the target space to the maximum extent, which is called “Polarization SR” (PSR) here.

In the process of obtaining PSR imaging, the total amount of information is expanded to four times that of the original measurement process. It should be noted that the expansion of this information amount is based on actual measurements, and the data are authentic.

2.4.2. Proposed method of PSR

Here, we propose a method for reaching PSR by using microscanning technology. The core idea is to make the detector or the image

Fig. 5. Schematic of polarization SR data restoration. The left image shows the original measurement data from a DoFP; the right image shows the data after polarization SR reconstruction.

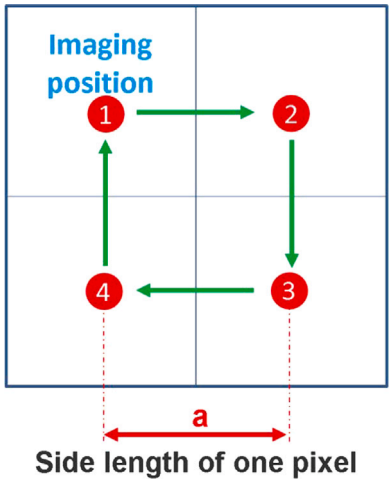

Fig. 6. Schematic of the relative displacement period between the image plane and detector.

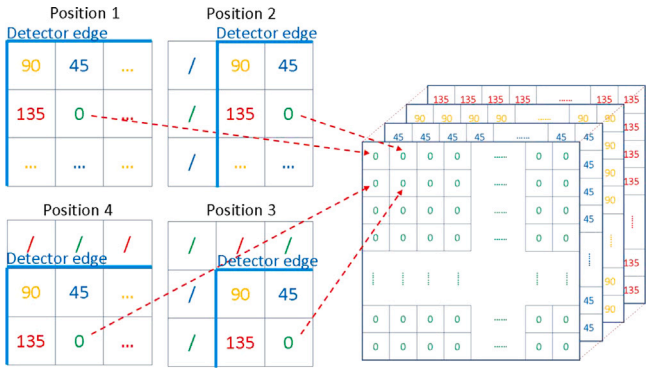

Fig. 7. Full-resolution sub-polarization image reconstruction method.

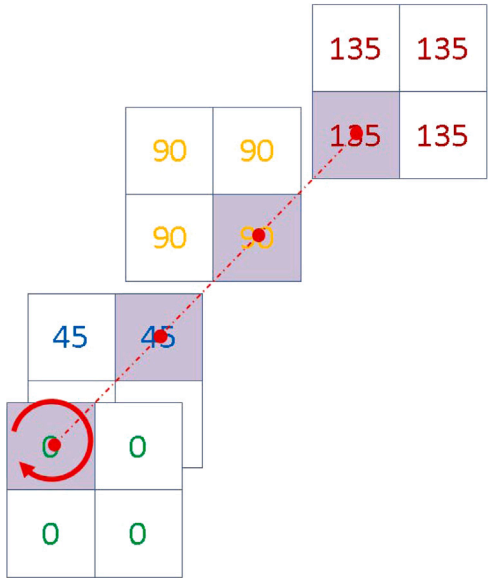

Fig. 8. Data space relative position relation diagram for calculating a polarization information pixel.

plane to follow the same trajectory as the cycle sequence of the four polarization states, and the exposure data are collected to fill in the originally lost sub-polarization information.

The specific implementation method is as follows.

A. Perform the pixel scale movement between the target scene image and the detector. A high-speed microscanning device is integrated in the optical system, which drives the optical elements or detectors to move in a square track as shown in Fig. 6.

B. For each of the four positions of the scanning device acquire a polarization image. It is necessary that the relative position of the image plane and the polarization detector should move by one pixel after each movement. After moving, it has a stable spatial relationship, and the retention time of this positional relationship should be longer than one exposure time, and four exposures constitute a complete data acquisition cycle.

C. Recombine the four acquired images along one data acquisition cycle to form four SR images each one containing information about only one polarization direction. In Fig. 7, the 0° polarization direction image is shown as an example. The filling method of the four pixels in the top left corner is shown in Fig. 7. The same procedure is followed for the other three polarization directions. At this time, we have four full resolution images, each one containing the information of a polarization detector, and the description of polarization information is no longer a simple image, but a three-dimensional data cube.

D. It should be noted that the images obtained in step C are spatially shifted by 1 pixel, as shown in Fig. 8,. Then, before the evaluation of any polarization parameter, the correct positioning of the images should be performed.

E. Generate polarization information images corresponding to the different polarization parameters of interest. For instance, considering Dolp image as an example, the Stokes vector is first calculated by Eq. (1). Assuming that the focal plane detector cannot detect the circular polarization information, S3 is ignored, and the polarization degree image is calculated according to Eq. (2). The restoration process is illustrated in Fig. 9.

2.5. Construction of polarization microscanning system

To implement PSR, we integrate the microscanning device with the optical lens and we select the aperture stop and its nearby lens to integrate with the microscanning device. When the microscanning device drives the aperture stop group to move step by step, the image plane also moves with it, and the detector position is relatively fixed, thus performing the relative shift between the detector and the conjugate image of the target scene. The optical system diagram is shown in Fig. 10:

The optical system is designed with a fixed focal length (19.7 mm) and a field of view angle of 24°×20°. The microscanning shifting device is integrated with the optical lens, and an imaging sensor with Sony

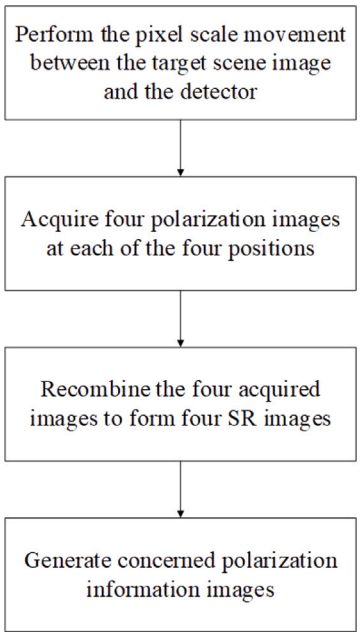

Fig. 9. Division-of-focal-plane polarization detection information recovery flowchart.

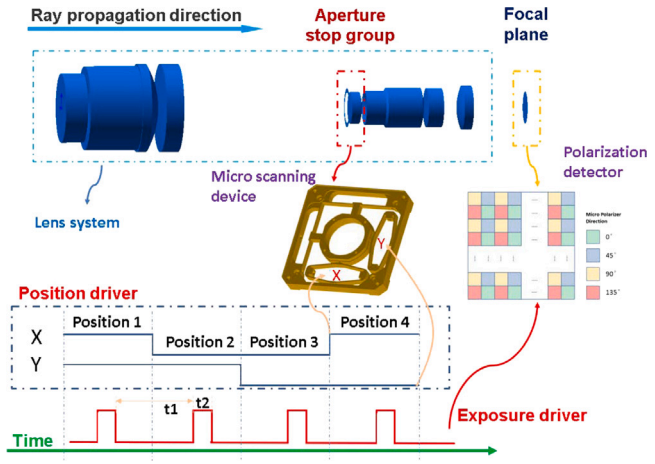

Fig. 10. Schematic of microscanning cooperative imaging system.

IMX250MYR polarization imaging chip is used as the detector. Simultaneously, it is equipped with a synchronizer drive controller to ensure that the detector acquires the image when the microscanning device is in the correct position. t1 represents the preparation time, during which the Microscanning device drives the aperture stop group to move to the right position and remain stable; t2 stands for integration time, during which the detector turns on exposure mode and acquires a polarized image of the target scene. Four integration times form an imaging cycle, acquire the basic image data, and calculate the full-resolution polarized image data cube of the target scene.

2.6. Calibration of the relative shifts

The focal plane polarization sensing technology needs to be accurate to the size of 1 pixel. Considering Sony's IMX250MZR polarization chip as an example, the center distance between two photosensitive pixels is 3.45 μm, which introduces very high requirements for the scanning accuracy of image position. Therefore, it is very important to calibrate the system to get the right "voltage-position" relationship. Every displacement between the image plane and the detector should

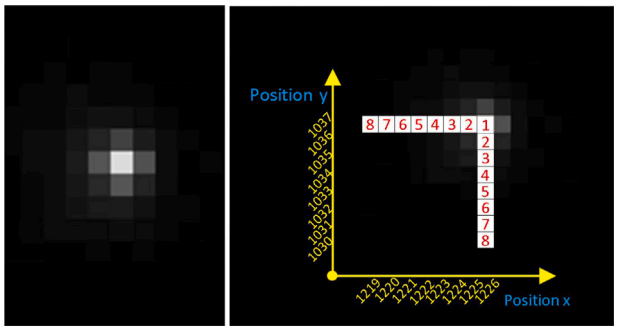

Fig. 11. Spot intensity distribution of parallel light on the detector and the track change in the calibration process.

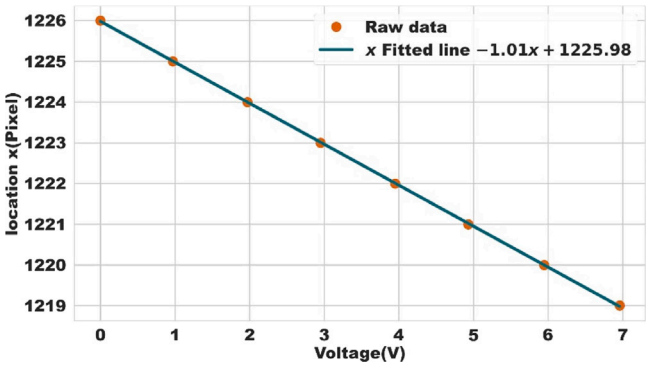

Fig. 12. Position vs voltage fitting curve along the x-axis, $[a_x, b_x] = [-1.01, 1225.98]$.

be accurate to one pixel, which determines the relative position accuracy of pixels in the polarization reconstructed image. We use the least square method to accurately calibrate the driving voltage of a single pixel. The specific calibration process is as follows.

1. Choose a collimated non polarized beam to enter the integrated optical imaging system, then will form an Airy spot on the target surface of the detector. As the beam has non-polarization characteristics all the polarization detectors will respond in the same way, in consequence, the optical system forms a cross-like pattern on the target surface, and the light intensity of the central pixel is the highest, as shown in Fig. 11;

2. Set the actual voltage to 0 V, adjust the incident angle of the beam so that the spot is near the center of the detector, and record the pixel position P at this time.

3. When changing the input voltages in the X and Y directions of the microscanning device, the light spot on the image plane of the detector starts to move. Every time it moves to the center of the next pixel, record the applied voltage V and pixel position P.

4. By considering the X direction as an example, and by increasing the voltage from 0 V to almost maximum input voltage, while the center position changes by N pixels. Observing the center position with naked eye results in errors. Therefore, we use the least square method to fit the relationship between "voltage V and position P" to a linear function $P = a_x V_x + b_x$ and obtain the slope a_x of the voltage curve, where a_x is the inverse of the voltage increment needed to move the spot one pixel.

5. Similarly, we repeat the above process to fit the Y direction and obtain a_y and b_y.

The X-axis calibration is shown in Fig. 12. The slope a_x and intercept b_x equals $[-1.01, 1225.98]$.

The Y-axis calibration is shown in Fig. 13. The slope a_y and intercept b_y equals $[-1.02, 1037.01]$.

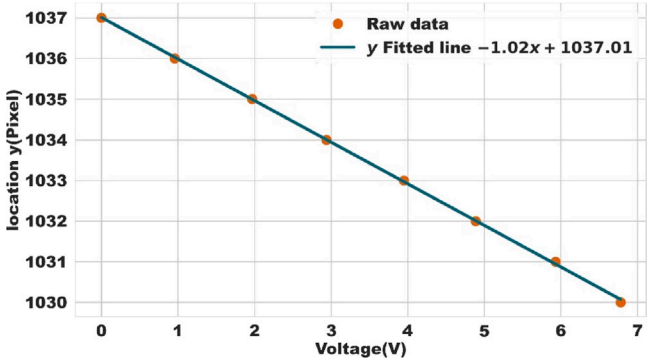

Fig. 13. Position vs Voltage fitting curve along the y-axis, $[a_y, b_y] = [-1.02, 1037.01]$.

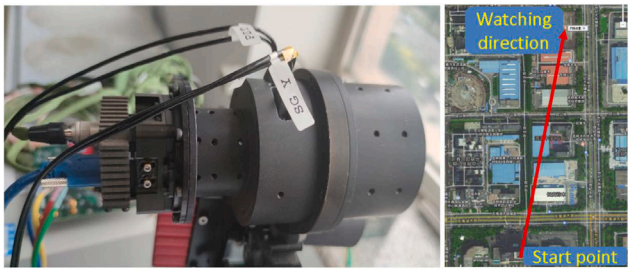

Fig. 14. PSR camera module and imaging orientation.

3. Experimental verification of PSR imaging in external field

3.1. System layout

As shown in Fig. 14, we construct an PSR imaging system and capture the image to the north through the window. The target scene mainly include the sky, buildings, trees, and cranes. The distance of a typical target crane is about 750 m.

3.2. Effect of improving spatial resolution

We use the aforementioned SR restoration system to obtain the original polarization data image, and reconstruct and restore the original data by using the method described in Section 2, to obtain four full-resolution linear polarization state image data of 0°, 45°, 90°, and 135°, which are twice the spatial resolution of the original single exposure data, and achieve SR on the pixel scale, as shown in Fig. 15.

Details of a crane obtained with the single exposure method is shown in Fig. 16. We can observe that the original images with low spatial resolution have lost considerable amount of detailed information: the characters on the crane cannot be recognized.

In Fig. 17 the details of the same crane obtained with the proposed method is shown. We can observe that the simple Chinese characters on the crane.

Once we have calculated the four SR images with the proposed method, we can evaluate any polarization parameter. For instance, in Fig. 18 we show the Degree of Linear Polarization (DoLP). On the left a gray level DoLP image is shown. To improve the visualization, on the right the same image using a "heat map" is shown.

To better visualize the improvement in resolution obtained with the proposed method, we consider some details of a building. Intensity images and DoLP images are provided to discuss the improvement of contrast and resolution. The details are listed in Table 1.

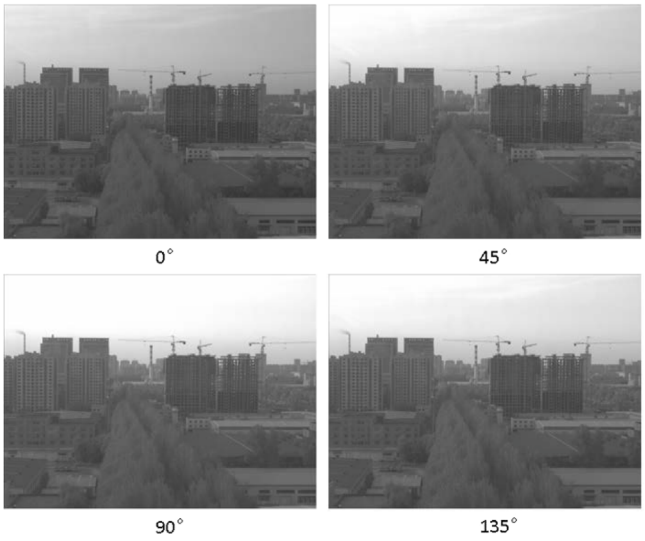

Fig. 15. Reconstructed "0°, 45°, 90°, and 135°" full-resolution linear polarization image data.

Fig. 16. Partial picture of the original image with 0° polarization direction.

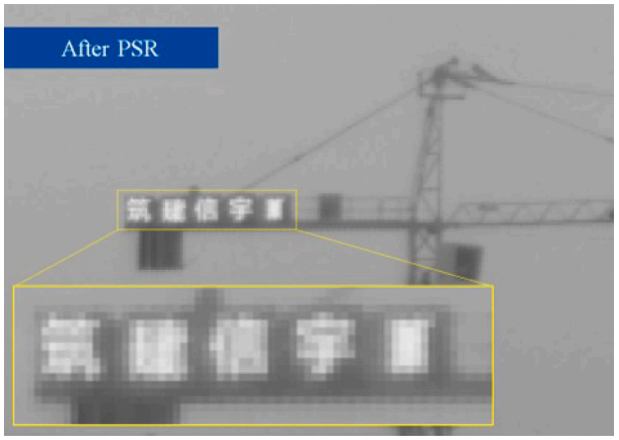

Fig. 17. Super-resolution image obtained with PSR method with 0° polarization direction.

Table 1
Comparison of the building details before and after PSR.

	A.Air conditioner	B.Building texture	C.Roof tile texture	Characteristics
1.90°polarization image before PSR	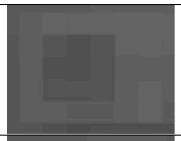		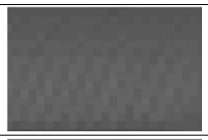	1.The image is relatively dim, and the image contrast is insufficient; 2.Insufficient details.
2.PSR 90° polarization image	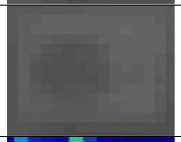		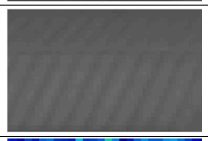	1.The image is relatively dim, and the image contrast is insufficient; 2.Image detail is enhanced.
3.DoLP image before PSR	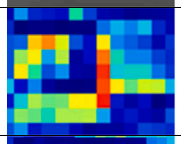	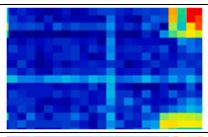	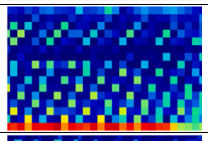	1.Image contrast is enhanced; 2.Insufficient details; 3.Error occurs in Dolp image.
4.PSR DoLP image	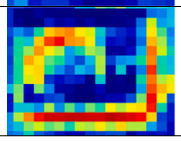	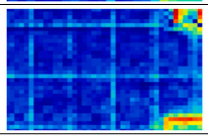	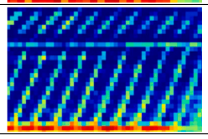	1.Image contrast is enhanced; 2.More detailed; 3.Error in Dolp image is corrected.

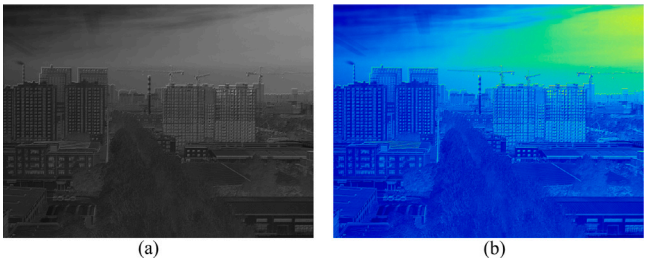

Fig. 18. PSR DoLP image. (a) Original PSR DoLP image; (b) heat map of PSR DoLP image.

3.3. Comparison of different super-resolution methods

Here, in order to objectively evaluate the influence of PSR technology on the amount of target scene information obtained, we use a no-reference method to analyze the above results. First of all, at the pixel scale, the polarization of the super-resolved image is 4 times that of the previous one, which makes the super-resolution image itself have a pixel advantage; However, in order to objectively evaluate the super-resolution results, we use the Nearest-neighbor Interpolation (NNI) method to expand the pixel scale of the original polarization image to be the same as that of the super-resolution results, and at the same time, we use bilinear method, bicubic spline method, gradient based interpolation method and correlation based method to perform super-resolution restoration of the original low-resolution image. In order to fully represent the ability of different methods to restore spatial details, this paper shows the results of different super-resolution polarization imaging applied to the same scene, as shown in Fig. 19.

Firstly, we can find from the above six images that the super-resolution method proposed in this paper has obvious advantages in expressing the target details, especially for the imaging of vertical window bars, the method proposed in this paper is clearer than other methods; Secondly, we evaluate the super-resolution results objectively based on six indicators such as grayscale mean (Mean), standard deviation (Std), information entropy (Entropy), spatial frequency (SF), image contrast (Contrast) and average gradient (AG). The evaluation results are shown in Table 2. The evaluation showed that the PSR method is equivalent to other methods in gray mean, standard deviation and information entropy. In the other three indexes of spatial

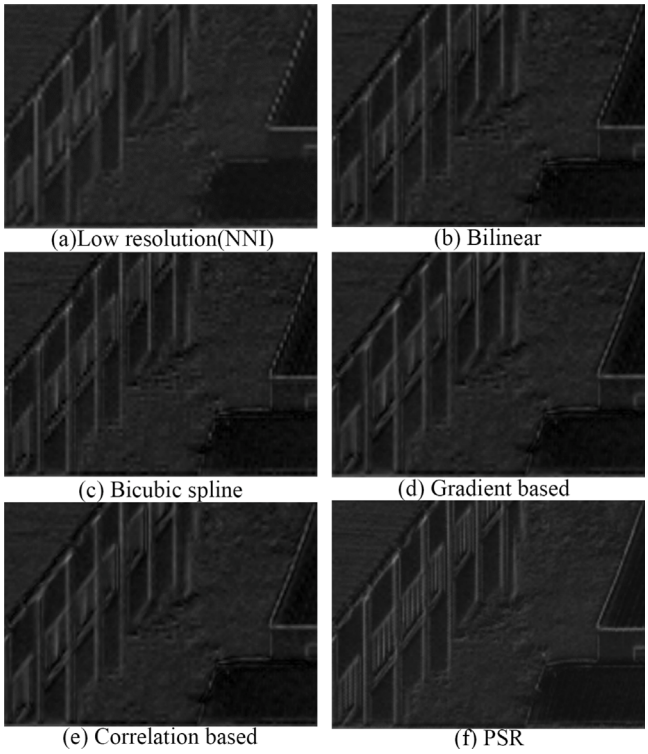

Fig. 19. Super-resolution effects between Dolp images obtained by different methods, figure (a) is the original low spatial resolution image; figure (b)–(e) are the four existing super-resolution method's results; figure (f) is the PSR method proposed in this paper.

frequency, image contrast and average gradient, the PSR method has obvious advantages compared with the bicubic spline method, which is the best method among other methods, increasing by 29%, 66% and 29% respectively. Other established methods are based on calculations rather than actual accurate measurements, so no matter how good the methods are, they are difficult to match the information obtained from actual measurements. It can be seen that the method proposed in this paper increases the amount of new information, effectively makes up for the disadvantages of DOFP polarization detector, and provides new

Table 2
The PSR method improves the amount of information in the image.

Indicator	NNI	Bilinear method	Bicubic spline	Gradient based	Correlation based	PSR	Enhancement
Mean	64.44	61.48	61.54	59.70	61.56	64.33	Equivalent
Std	31.07	31.80	31.81	31.04	31.91	31.49	Equivalent
Entropy	6.68	6.73	6.74	6.69	6.74	6.71	Equivalent
SF	8.25	9.25	9.97	8.97	9.58	12.87	+29%
Contrast	34.04	42.78	49.76	40.22	45.91	82.85	+66%
AG	0.0029	0.0032	0.0035	0.0031	0.0033	0.0045	+29%

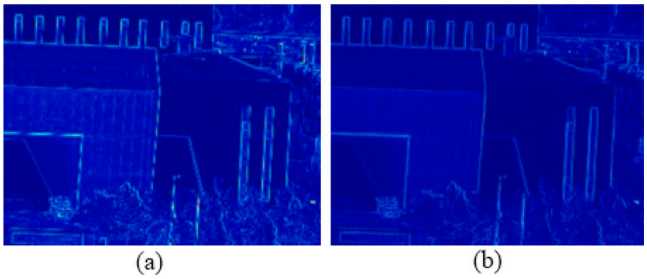

Fig. 20. Suppression of low-resolution linear discontinuity problems by super-resolution technology; (a) a color representation of the Dolp image obtained from the original low-resolution image; (b) the image after resolution restoration is achieved by applying the method proposed herein. (For interpretation of the references to color in this figure legend, the reader is referred to the web version of this article.)

technical support for richer and more accurate polarization remote sensing information acquisition.

3.4. Effect of low-resolution linear discontinuity

Low-resolution images tend to lead to linear discontinuity, a phenomenon that also persists in polarization images. In order to verify the inhibitory effect of super-resolution technology on this phenomenon, this paper uses the proposed PSR technology to carry out imaging of buildings with typical linear characteristics, and the images before and after super-resolution are shown in Fig. 20. In the acquired images, we find that the original intermittent straight line structure is well restored.

4. Discussion

In this paper, aiming to overcome the disadvantages of spatial resolution reduction DoFP detector and introduction of errors in polarization information calculation, a new idea of obtaining polarization SR remote sensing by combining a microscanning device with the traditional optical system is proposed. Polarization image restoration method and polarization information calculation method are also provided. The core idea of this new method is described as follows. Firstly, the pixel-level translational microscanning is performed between the image plane and the detector, and the full resolution image with 0°, 45°, 90°, and 135° linear polarization angles are restored by dislocation extraction. Subsequently, according to the calculated four polarization state images, the DoLP images are obtained.

4.1. Discussion on polarization super-resolution images

Here, we discuss the effect of this method according to Table 1. For the convenience of discussion, we use the combination of numbers 1–4 and letters A–C in the table for comparative analysis. The method introduced in this paper has the following characteristics:

1. The spatial details of the target are more abundant. By comparing the images in the 1st and 2nd rows, it can be observed that the pixels in the first row are larger, while the pixels in the second row are relatively more delicate. Especially, compared with image 2A, in image 1A, the original circular air-conditioning exhaust fan is represented as a square by low-resolution pixels, while in image 2A, its circular feature is restored.

2. Polarized images have a significant effect on man-made targets. The intensity images in the 1st 2nd rows are relatively dim due to the detector integration time and illumination intensity. However, in the polarization image, the contrast is visibly enhanced.

3. DoLP image has visible prominent effect on the texture of the object. In 1B and 2B, the texture of the building is very dim, which makes it difficult for human eyes to identify, while in 3B and 4B, the lattice texture of the building can be clearly imaged, and especially after applying this PSR method, the texture is clearer. The roof tiles depicted in group C also have similar effects. So, by using the DoLP more contrasted images are obtained. And in both cases (intensity and DoLP) we can appreciate the improvement in the resolution when the proposed method is used.

4. The errors and missing information in the low-resolution DoLP images are corrected in the PSR image. In Fig. 3A, the edge of the air conditioner is not displayed, but its outline is better shown in Fig. 4A. Fig. 4B compensates for the missing texture information in 3B. In Fig. 3C, the tiles' stripes have been interrupted, and the roof part is not shown, which is a typical error in texture interpretation. However, in Fig. 4C, this error is well compensated. In summary, in Table 1, we can observe that the picture of 90° intensity polarized image before PSR is dim, the contrast of the image is insufficient, and the expressive force of details is insufficient. The detail expression of the 90° intensity polarized image after PSR is significantly improved, but the low illumination image is still relatively dim and the image contrast is insufficient. The contrast of DoLP image before PSR is improved, but the spatial resolution is insufficient, and DoLP calculation error exists. After PSR, the contrast of DoLP image is visibly improved, the expressive force of image details is also improved, and the calculation error of DoLP is suppressed.

In summary, in Table 1, we can observe that the picture of 90° intensity polarized image before PSR is dim, the contrast of the image is insufficient, and the expressive force of details is insufficient. The detail expression of the 90° intensity polarized image after PSR is significantly improved, but the low illumination image is still relatively dim and the image contrast is insufficient. The contrast of DoLP image before PSR is improved, but the spatial resolution is insufficient, and DoLP calculation error exists. After PSR, the contrast of DoLP image is visibly improved, the expressive force of image details is also improved, and the calculation error of DoLP is suppressed.

4.2. Discussion on the characteristics of the PSR method

1. Super-resolution data has accuracy. From the comparation parts, we can learn that the method proposed in this paper has obvious advantages over other existing methods, because the PSR method does not rely on empirical formulas, does not depend on the amount of training data, and is completely based on actual measurement, which is significantly different from the deep learning method relying on the training sample library, so the PSR method has a wider applicability. And at the same time, the PSR method has the possibility of becoming the reference for other polarization super-resolution algorithms. This property makes it more feasible to use deep learning methods to improve the spatial resolution of DoFP polarimeters in real time.

2. The PSR algorithm suppresses linear discontinuities in DOLP images. In the section "Effect of low-resolution linear discontinuity", we give the compensation effect of PSR on the linear discontinuity phenomenon, which is a direct application of proposed method. Image information closer to the real situation is conducive to the subsequent development of super-resolution technology based on deep learning.

3. Limitations of the PSR algorithm. It should be acknowledged that the PSR algorithm still has its limitations, especially in the process of super-resolution information restoration of dynamic scenes, many factors need to be reconsidered, such as the observer needs to achieve stable tracking of the target, or obtaining information such as the relative motion speed between the object and the observer, the observation distance, etc., when the observer captures the target, the PSR method can work at each snapshot image in combination with its previous three images, and this requires close combination with high-speed computational imaging technology.

5. Conclusions

In this paper we propose a new method to increase the spatial resolution of a DoFP polarization sensor, while eliminating the calculation error of polarization information caused by the spatial separation of the different polarization sensors. The method uses a DoFP polarization sensor with a microscanning device.

In this study, the basic concept of PSR is put forward, and the basic principle, system structure, calibration process and application for external imaging are introduced. We have achieved a 2-fold increase in each direction in the resolution of the original linear polarization images and, consequently, of all the parameters extracted from them like the DoLP. This method eliminates the calculation error caused by the loss of spatial information in the original calculation method.

Because high resolution and accurate information restoration are very important to people, especially in areas with strict requirements on volume and weight, such as Ad Astra, aerial remote sensing, life science, etc., PSR technology may make irreplaceable contributions.

In short, the polarization super-resolution technology proposed in this paper makes up for the problems of spatial resolution loss and information solving errors on the basis of ensuring the advantages of the DoFP polarization sensor as much as possible, and it is believed that this technology is expected to have a positive effect in the field of polarimetric Earth Observation Remote Sensing.

Next, it is necessary to carry out in-depth research on the parts of ultra-resolution remote sensing of moving targets, and it is also meaningful to achieve 3x or 4x times higher spatial resolution polarization images.

CRediT authorship contribution statement

Dong Yao: Conceive the basic idea, Writing – original draft. **Hangang Liang:** Data processing. **Juan Campos:** Methodology, Manuscript revision. **Lei Yan:** Conceptualization, Methodology. **Chunhui Yan:** Methodology, Experimental operation. **Chunming Jiang:** Writing – review & editing. **Songnian Tan:** Instrument system construction. **Chao Liang:** Control system construction. **Hanyu Wang:** Data analysis. **Lingtong Meng:** Methodology, Experimental operation. **Yanping Cheng:** Instrument system construction.

Declaration of competing interest

The authors declare that they have no known competing financial interests or personal relationships that could have appeared to influence the work reported in this paper.

Data availability

The authors do not have permission to share data.

Acknowledgments

We gratefully acknowledge National Key Research and Development Program (2022YFC2807400), Chinese Academy of Sciences (8091A140309, CXJJ-20S04), National Natural Science Foundation of China (61905242) for funding this work.

References

Altaqui, et al., 2021. Mantis shrimp–inspired organic photodetector for simultaneous hyperspectral and polarimetric imaging. Sci. Adv. 7 (10), eabe3196.
Aron, Y., Gronau, Y., 2005. Polarization in the MWIR: a method to improve target aquisition. In: Infrared Technology and Applications XXXI, Vol. 5783. SPIE, pp. 653–661.
Atkinson, G.A., O'Hara Nash, S., Smith, L.N., 2021. Precision fibre angle inspection for carbon fibre composite structures using polarisation vision. Electronics 10 (22), 2765.
Azzam, R., 1985. Arrangement of four photodetectors for measuring the state of polarization of light. Opt. Lett. 10 (7), 309–311.
Barter, J.D., Lee, P.H., Thompson Jr., H., Schneider, T., 1997. Stokes parameter imaging of scattering surfaces. In: Polarization: Measurement, Analysis, and Remote Sensing, Vol. 3121. SPIE, pp. 314–320.
Born, M., Wolf, E., 2013. Principles of Optics: Electromagnetic Theory of Propagation, Interference and Diffraction of Light. Elsevier.
Cairns, B., Russell, E.E., LaVeigne, J.D., Tennant, P.M., 2003. Research scanning polarimeter and airborne usage for remote sensing of aerosols. In: Polarization Science and Remote Sensing, Vol. 5158. SPIE, pp. 33–44.
Chen, J., Li, Y., Cao, L., 2021. Research on region selection super resolution restoration algorithm based on infrared micro-scanning optical imaging model. Sci. Rep. 11 (1), 1–8.
Cronin, T.W., Shashar, N., Caldwell, R.L., Marshall, J., Cheroske, A.G., Chiou, T.-H., 2003. Polarization vision and its role in biological signaling. Integr. Comp. Biol. 43 (4), 549–558.
Egan, W.G., 1992. Polarization in remote sensing. In: Polarization and Remote Sensing, Vol. 1747. SPIE, pp. 2–48.
Farlow, C.A., Chenault, D.B., Pezzaniti, J.L., Spradley, K.D., Gulley, M.G., 2002. Imaging polarimeter development and applications. In: Polarization Analysis and Measurement IV, Vol. 4481. SPIE, pp. 118–125.
Gao, S., Gruev, V., 2011. Bilinear and bicubic interpolation methods for division of focal plane polarimeters. Opt. Express 19 (27), 26161–26173.
Gao, S., Gruev, V., 2012. Gradient based interpolation for division of focal plane polarization imaging sensors. In: 2012 IEEE International Symposium on Circuits and Systems. ISCAS, IEEE, pp. 1855–1858.
Gao, S., Gruev, V., 2013. Gradient-based interpolation method for division-of-focal-plane polarimeters. Opt. Express 21 (1), 1137–1151.
Goldstein, D.H., 2000. Polarimetric characterization of federal standard paints. In: Polarization Analysis, Measurement, and Remote Sensing III, Vol. 4133. SPIE, pp. 112–123.
Graps, A., Lane, A., 1986. Voyager 2 photopolarimeter experiment: Evidence for tenuous outer ring material at Saturn. Icarus 67 (2), 205–210.
Gruev, V., Perkins, R., York, T., 2010a. CCD polarization imaging sensor with aluminum nanowire optical filters. Opt. Express 18 (18), 19087–19094.
Gruev, V., Van der Spiegel, J., Engheta, N., 2010b. Dual-tier thin film polymer polarization imaging sensor. Opt. Express 18 (18), 19292–19303.
Harnett, C.K., Craighead, H.G., 2002. Liquid-crystal micropolarizer array for polarization-difference imaging. Appl. Opt. 41 (7), 1291–1296.
Iannarilli Jr., F.J., Shaw, J.A., Jones, S.H., Scott, H.E., 2000. Snapshot LWIR hyperspectral polarimetric imager for ocean surface sensing. In: Polarization Analysis, Measurement, and Remote Sensing III, Vol. 4133. SPIE, pp. 270–283.
Jacques, S.L., Ramella-Roman, J.C., Lee, K., 2002. Imaging skin pathology with polarized light. J. Biomed. Opt. 7 (3), 329–340.
Kudenov, M.W., Pezzaniti, J.L., Gerhart, G.R., 2009. Microbolometer-infrared imaging Stokes polarimeter. Opt. Eng. 48 (6), 063201.
Labhart, T., 1988. Polarization-opponent interneurons in the insect visual system. Nature 331 (6155), 435–437.
Lillie, C.F., Hord, C.W., Pang, K., Coffeen, D.L., Hansen, J.E., 1977. The Voyager mission photopolarimeter experiment. Space Sci. Rev. 21 (2), 159–181.
Liu, Y., York, T., Akers, W.J., Sudlow, G.P., Gruev, V., Achilefu, S., 2012. Complementary fluorescence-polarization microscopy using division-of-focal-plane polarization imaging sensor. J. Biomed. Opt. 17 (11), 116001.
LotharSchermelleh, A., ThomasHuser, C., MarkusSauer, O.B., Gregor, P., 2019. Drummen. Super-resolution microscopy demystified. Nature Cell Biol. 21 (1), 72–84.
Lythgoe, J.N., Hemmings, C., 1967. Polarized light and underwater vision. Nature 213 (5079), 893–894.
Momeni, M., Titus, A.H., 2006. An analog VLSI chip emulating polarization vision of octopus retina. IEEE Trans. Neural Netw. 17 (1), 222–232.

Nordin, G.P., Meier, J.T., Deguzman, P.C., Jones, M.W., 1999. Diffractive optical element for Stokes vector measurement with a focal plane array. In: Polarization: Measurement, Analysis, and Remote Sensing II, Vol. 3754. SPIE, pp. 169–177.

Perkins, R., Gruev, V., 2010. Signal-to-noise analysis of Stokes parameters in division of focal plane polarimeters. Opt. Express 18 (25), 25815–25824.

Pezzaniti, J.L., Chenault, D.B., 2005. A division of aperture MWIR imaging polarimeter. In: Polarization Science and Remote Sensing II, Vol. 5888. Spie, pp. 239–250.

Ratliff, B., Lacasse, C., Tyo, J., 2009. Quantifying ifov error and compensating its effects in dofp polarimeters. Opt. Express 17 (11), 9112–9125.

Roche, M.E., Chenault, D.B., Vaden, J.P., Lompado, A., Voelz, D., Schulz, T.J., Givens, R.N., Gamiz, V.L., 2010. Synthetic aperture imaging polarimeter. In: Polarization: Measurement, Analysis, and Remote Sensing IX, Vol. 7672. SPIE, pp. 58–69.

Sarkar, M., Bello, D.S.S.S.S., Van Hoof, C., Theuwissen, A., 2010. Integrated polarization analyzing CMOS image sensor for material classification. IEEE Sens. J. 11 (8), 1692–1703.

Solomon, J.E., 1981. Polarization imaging. Appl. Opt. 20 (9), 1537–1544.

Sweeney, A., Jiggins, C., Johnsen, S., 2003. Polarized light as a butterfly mating signal. Nature 423, 31–32.

Tyo, J.S., 2006. Hybrid division of aperture/division of a focal-plane polarimeter for real-time polarization imagery without an instantaneous field-of-view error. Opt. Lett. 31 (20), 2984–2986.

Tyo, J.S., LaCasse, C.F., Ratliff, B.M., 2009. Total elimination of sampling errors in polarization imagery obtained with integrated microgrid polarimeters. Opt. Lett. 34 (20), 3187–3189.

Valli, J., Garcia-Burgos, A., Rooney, L.M., e Oliveira, B.V.d.M., Duncan, R.R., Rickman, C., 2021. Seeing beyond the limit: A guide to choosing the right super-resolution microscopy technique. J. Biol. Chem. 297 (1).

Walraven, R., 1981. Polarization imagery. Opt. Eng. 20 (1), 14–18.

Wolff, L.B., 1997. Polarization vision: a new sensory approach to image understanding. Image Vis. Comput. 15 (2), 81–93.

York, T., Gruev, V., 2012. Characterization of a visible spectrum division-of-focal-plane polarimeter. Appl. Opt. 51 (22), 5392–5400.

Zeng, X., Chen, H., Luo, Y., Ye, W., 2019a. Automated diabetic retinopathy detection based on binocular siamese-like convolutional neural network. IEEE Access 7, 30744–30753.

Zeng, X., Luo, Y., Zhao, X., Ye, W., 2019b. An end-to-end fully-convolutional neural network for division of focal plane sensors to reconstruct s 0, dolp, and aop. Opt. Express 27 (6), 8566–8577.

Zhang, X., Huang, W., Xu, M., Jia, S., Xu, X., Li, F., Zheng, Y., 2019b. Super-resolution imaging for infrared micro-scanning optical system. Opt. Express 27 (5), 7719–7737.

Zhang, J., Luo, H., Hui, B., Chang, Z., 2016. Image interpolation for division of focal plane polarimeters with intensity correlation. Opt. Express 24 (18), 20799–20807.

Zhang, W., Ma, L., Zhao, L., Cao, Y., 2019a. Real-time sky polarized light navigation based on micropolarized array imaging. Transducer Microsyst. Technol. 38, 9–11.

Zhang, J., Shao, J., Luo, H., Zhang, X., Hui, B., Chang, Z., Liang, R., 2018. Learning a convolutional demosaicing network for microgrid polarimeter imagery. Opt. Lett. 43 (18), 4534–4537.

Zhang, J., Ye, W., Ahmed, A., Qiu, Z., Cao, Y., Zhao, X., 2017. A novel smoothness-based interpolation algorithm for division of focal plane polarimeters. In: 2017 IEEE International Symposium on Circuits and Systems. ISCAS, IEEE, pp. 1–4.